doi:10.1016/j.ultrasmedbio.2004.07.009

● *Original Contribution*

ON THE POTENTIAL OF THE LAGRANGIAN SPECKLE MODEL ESTIMATOR TO CHARACTERIZE ATHEROSCLEROTIC PLAQUES IN ENDOVASCULAR ELASTOGRAPHY: IN VITRO EXPERIMENTS USING AN EXCISED HUMAN CAROTID ARTERY

ROCH L. MAURICE,* ÉLISABETH BRUSSEAU,[†] GÉRARD FINET[‡] and GUY CLOUTIER*

*Laboratory of Biorheology and Medical Ultrasonics, Research Center, University of Montreal Hospital, Montreal, Québec, Canada: [†]CREATIS, UMR CNRS 5515, affiliated to INSERM, Lyon, France; and [‡]Department of Hemodynamics, Cardiovascular Hospital, Claude Bernard University, Lyon, France

Abstract—Endovascular ultrasound (US) elastography (EVE) was introduced to supplement endovascular US echograms in the assessment of vessel lesions and for endovascular therapy planning. Indeed, changes in the vascular tissue stiffness are characteristic of vessel wall pathologies and EVE appears as a very appropriate imaging technique to outline the elastic properties of vessel walls. Recently, a model-based approach was proposed to assess tissue motion in EVE. It specifically consists of a nonlinear minimization algorithm that was adapted to speckle motion estimation. Regarding the theoretical framework, such an approach considers the speckle as a material property; this assumption then led to the derivation of the optical flow equations, which were suitably combined with the Lagrangian speckle model estimator to provide the full 2-D polar strain tensor. In this study, the proposed algorithm was validated in vitro using a fresh excised human carotid artery. The experimental setup consisted of a cardiovascular imaging system (CVIS) US scanner, working with a 30-MHz mechanical rotating single-element transducer, a digital oscilloscope and a pressuring system. A sequence of radiofrequency (RF) images was collected while incrementally adjusting the intraluminal static pressure steps. The results showed the potential of this 2-D algorithm to characterize and to distinguish an atherosclerotic plaque from the normal vascular tissue. Namely, the geometry as well as some mechanical characteristics of the detected plaque were in good agreement with histology. The results also suggested that there might exist a range of intraluminal pressures for which plaque detectability is optimal. (E-mail: guy.cloutier@umontreal.ca)   © 2005 World Federation for Ultrasound in Medicine & Biology.

Key Words: Endovascular elastography, Lagrangian speckle model estimator, Vascular imaging, Vulnerable plaque, Arterial disease, Atherosclerosis.

INTRODUCTION

Atherosclerosis, which is a disease of the intima layer of arteries, remains a major cause of mortality in western countries. This pathology is characterized by a focal accumulation of lipids, complex carbohydrates, blood cells, fibrous tissues and calcified deposits, forming a plaque that thickens and hardens the arterial wall. A severe complication of atherosclerosis is thrombosis, a consequence to plaque rupture or fissure, that might lead, according to the event localization, to unstable angina, brain or myocardial infarction and sudden ischemic death (Falk 1989; Davies and Thomas 1985; Zaman et al. 2000). Plaque rupture is a complicated mechanical process, correlated with plaque morphology, composition, mechanical properties and with the blood pressure and its long-term repetitive cycle (Fung 1993; Falk 1992). Extracting information on the plaque local mechanical properties and on the surrounding tissues may thus reveal relevant features about plaque vulnerability (Fisher et al. 2000; Ohayon et al. 2001). Unfortunately, no imaging modality currently in clinical use allows the access to these properties.

Endovascular elastography (EVE)

So far, diagnosis and prognosis of atherosclerosis evolution mainly rely on plaque morphology and vessel

Address correspondence to: G. Cloutier, Ph.D., Director of the Laboratory of Biorheology and Medical Ultrasonics, Research Center, University of Montreal Hospital, 2099 Alexandre de Sève (room Y-1619), Montréal, Québec H2L 2W5 Canada. E-mail: guy.cloutier@umontreal.ca

stenosis degree. This information can accurately be accessed with intravascular ultrasound (US), or IVUS, imaging because this modality provides high-resolution cross-sectional images of arteries. Accurate quantitative analysis of the disease is thus easily performed by precise measurements of the lumen area, arterial dimensions and dimensions specific to the plaque. Moreover, IVUS permits the qualitative characterization of plaque components but, roughly, in terms of fatty, fibrous or calcified plaques and with possible misinterpretations. This makes IVUS alone, insufficient to predict the plaque mechanical behavior. However, elastic properties of vessel walls can be derived from radiofrequency (RF) IVUS images, by integrating elastographic processing methods. Indeed, endovascular US elastography (EVE) is an in-development imaging technique that aims to outline elastic properties of vessel walls. Its principle consists of acquiring sequences of cross-sectional vessel US images, while the vascular tissue is compressed by applying a force from within the lumen. Strain distribution is then estimated by tracking, from the signals, the modifications induced by the stress application. In practice, in EVE, such a stress can be induced by the normal cardiac pulsation or by using a compliant intravascular angioplasty balloon.

1-D tissue-motion assessment in EVE

Several approaches have been proposed to assess tissue motion in EVE. Whereas 1-D motion estimators are likely more sensitive to pre- and postmotion signal decoherence, 2-D motion estimators are expected to be more reliable. However, the most commonly used motion estimators in EVE applications are 1-D correlation-based techniques. This choice is mainly dictated by the ability of such estimators to be implemented; they also may provide real-time tissue motion estimates. In 1-D correlation-based tissue motion estimators, the displacement between pre- and postmotion pairs of RF lines is determined using cross-correlation analysis. This technique was used to investigate EVE feasibility on vessel-mimicking phantoms (de Korte et al. 1997), on excised human femoral and coronary arteries (de Korte et al. 1998, 2000a), and in vivo on human coronary arteries (de Korte et al. 2000b).

A different implementation of the 1-D cross-correlation technique was proposed by Brusseau et al. (2001) to investigate a post mortem human excised carotid artery. They computed an adaptive and iterative estimation of local scaling factors, using the phase information between pre- and postcompression RF signals. The authors suggested that this approach may be less sensitive to decorrelation noise than conventional 1-D correlation-based estimators. On the other hand, others also proposed to assess local scaling factors, but in the frequency domain (Talhami et al. 1994). They presented some initial in vitro and in vivo results that were obtained with this spectral tissue strain estimator. Envelope B-mode data were used in this last study. No further validation of the spectral approach was so far conducted in EVE.

2-D tissue motion assessment in EVE

In vivo applications of EVE are subjected to many difficulties. For instance, the position of the catheter in the lumen is generally neither in the center nor parallel to the vessel axis and the lumen geometry is generally not circular. In such conditions, tissue displacements may be misaligned with the US beam, introducing substantial decorrelation between the pre- and the post-tissue-compression signals. Regarding that, 1-D estimators may not be optimal if such decorrelation is not appropriately compensated for. Ryan and Foster (1997) then proposed to use a 2-D correlation-based speckle-tracking method to compute vascular elastograms. This approach was experimented on envelope B-mode data from in vitro vessel-mimicking phantoms. No further validation was, however, conducted by this group.

Another potential difficulty that is associated with EVE in vivo applications stems from the eventual cyclic catheter movement in the vessel lumen. Owing to the pulsatile blood flow motion, catheter instability may constitute another source of signal decorrelation between pre- and postcompression signals. To that, Shapo et al. (1996a, 1996b) proposed the use of an angioplasty balloon to stabilize the catheter in the vessel lumen. Tissue motion was assessed using a 2-D correlation-based phase-sensitive speckle-tracking technique. Preliminary results from simulations and from in vitro vessel-mimicking phantom investigations were presented; envelope B-mode data were used.

In addition to the above difficulties, the heterogeneous nature of the vascular tissue and of the plaque itself may induce very complex tissue deformations (nonrigid rotation, scaling, shear, etc.). Whereas most of the current elastographic methods use correlation techniques to assess tissue motion, they may not be optimal to investigate such complex strain patterns. Recently, the Lagrangian speckle model estimator (LSME) was proposed for strain computation in EVE (Maurice et al. 2004a). The LSME was then formulated in a polar coordinate system and the method was implemented through an adapted version of the Levenberg–Marquardt minimization algorithm to compute the full 2-D polar strain tensor. Interestingly, it was shown with simulations that the LSME might provide useful information about the heterogeneous nature of atherosclerotic plaques. In the current study, an in vitro experimentation of the adapted LSME is presented to validate the method.

MATERIALS AND METHODS

Experimental setup description

The experimental setup consisted in a CVIS (Clear-View, CardioVascular Imaging System Inc., Sunnyvale, CA) US scanner, working with a 30-MHz mechanical rotating single-element transducer, a digital oscilloscope (LECROY, model 9374L, Chestnut Ridge, NY) and a self-made pressuring system (Fig. 1). Artery extremities were fixed to two rigid sheaths by watertight connectors, separated according to the original longitudinal dimension of the vessel before excision. The intravascular catheter was introduced through the proximal sheath into the lumen of the artery and then through the distal sheath. The distal sheath was closed with a clamp to insure watertightness of the system. Because of the sheath rigidity and of the system watertightness, injecting fluid inside the system resulted in an increase of the pressure inside the arterial lumen. A syringe was then connected to the proximal sheath and the inner pressure was increased or decreased by manually varying the fluid volume (precision: $\Delta V = 0.01$ mL) inside the lumen. Whereas the quantitative pressure values were not monitored by an independent means, the fluid volume inside the lumen was maintained constant during each acquisition. The US probe was fixed approximately at the center of the arterial lumen by two guiding elements. This protocol was used to limit probe motion and accordingly to reduce geometrical artefacts (Delachartre et al. 1999).

Data acquisition

In vitro experiments with the carotid artery were performed at room temperature. At each static pressure step (volume step), a scan of 256 angles was performed. A set of 11 RF images was so acquired for consecutive increasing physiological fluid pressure levels. Sampling of the data was phase-synchronized, with the top image synchronizer and the RF signal synchronization (external outputs of the CVIS US scanner). The top image synchronizer allows the user to select an angular position from which the acquisition started; it thus permitted the acquisition of angularly aligned sets of images. The RF signal synchronization was done at the pulse-repetition frequency (PRF) of the bursts transmitted to the single-element transducer. RF data were digitized at a 500-MHz sampling frequency in 8 bits format, stored on a PCMCIA hard disk in the LeCroy oscilloscope and processed off-line.

The Lagrangian speckle model estimator

The Lagrangian speckle model estimator (LSME) that was used to compute the elastograms is described in detail elsewhere (Maurice et al. 2004a). Assuming a small region-of-interest (ROI) and a small tissue motion, it can mathematically be formulated as the following nonlinear minimization problem:

$$\underset{LT_p}{MIN} \|I(r, \phi, 0) - I_{Lag}(r, \phi, t)\|^2, \tag{1}$$

where (r,ϕ) defines the image coordinate system, and t
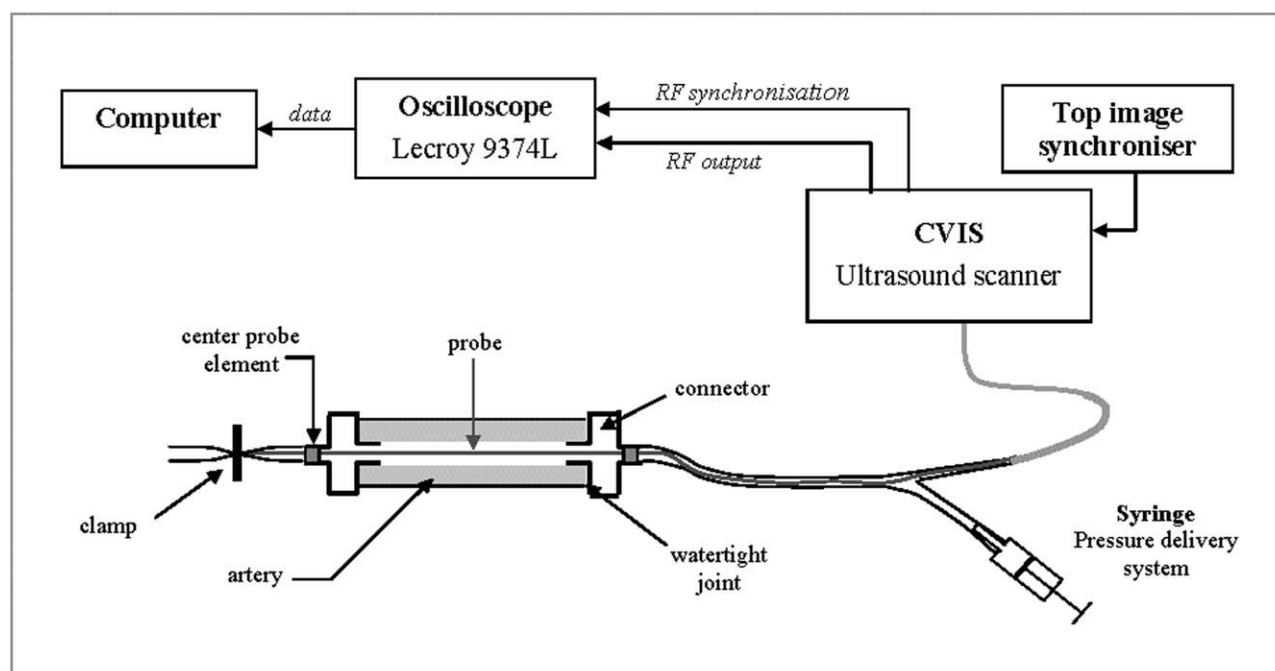
Fig. 1. Experimental setup for endovascular elastographic investigations.

indicates the time. $I(r,\phi,0)$ is the pre-tissue-motion RF image, and $I_{Lag}(r,\phi,t)$ is the Lagrangian speckle image (LSI) at time t. It is worth mentioning that the LSI is defined as a post-tissue-motion RF image that was numerically compensated for tissue motion, as to achieve the best match with $I(r,\phi,0)$ (Maurice and Bertrand 1999). The appellation "Lagrangian" refers to the Lagrangian description of motion. The minimum of eqn (1) was obtained using the appropriate $[LT_p]$, a 2-D linear transformation matrix associated with the polar coordinate system (r,ϕ).

As demonstrated by Maurice et al. (2004a), it is important to note that, for a small ROI $(\Delta r, \Delta\phi)$ being far from the lumen center, motion can equivalently be investigated using either the polar or the Cartesian coordinate system. In other words, the following approximation can be done:

$$\Delta = LT - I \cong LT_p - I, \qquad (2)$$

where Δ is defined as the Cartesian deformation matrix; LT is a 2-D linear transformation matrix associated with the Cartesian (x,y) coordinate system; I is the 2-D identity matrix; and LT_p, defined earlier, is a 2-D linear transformation matrix associated with the polar (r,ϕ) coordinate system. Furthermore, it is known that, for a small ROI, tissue motion can be approximated by an affine transformation; this can be expressed in Cartesian coordinates as:

$$\begin{bmatrix} p(x,y,t) \\ q(x,y,t) \end{bmatrix} = \underbrace{\begin{bmatrix} \theta_1 \\ \theta_4 \end{bmatrix}}_{Tr} + \underbrace{\begin{bmatrix} \theta_2 & \theta_3 \\ \theta_5 & \theta_6 \end{bmatrix}}_{LT} \begin{bmatrix} x \\ y \end{bmatrix}, \qquad (3)$$

where θ_i is a function of time t $(\theta_i(t))$. Equation (3) is the result of a translation of the center of the ROI (vector T_r) and of a linear geometrical transformation of coordinates (matrix $[LT]$, which is used to define rotation, scaling, shearing, etc.). Equation (3) can also be seen as trajectories that describe a tissue motion in a region of constant strain (Maurice and Bertrand 1999). Assuming that (u_x,u_y) represent the displacement field in the (x,y) coordinate system, $[LT]$ relates the strain tensor (ε) through the following relationships:

$$\begin{bmatrix} u_x \\ u_y \end{bmatrix} = \begin{bmatrix} p(x,y,t) - x \\ q(x,y,t) - y \end{bmatrix} = \begin{bmatrix} \theta_1 \\ \theta_4 \end{bmatrix} + \Delta \begin{bmatrix} x \\ y \end{bmatrix} \qquad (4a)$$

with

$$\Delta = \begin{bmatrix} \theta_2 - 1 & \theta_3 \\ \theta_5 & \theta_6 - 1 \end{bmatrix}, \qquad (4b)$$

$$\varepsilon_{ij}(t) = \frac{1}{2}\big[\Delta_{ij}(t) + \Delta_{ji}(t)\big]. \qquad (4c)$$

The radial strain then becomes equivalent to ε_{22} ($= \Delta_{22} = \theta_6 - 1$). The map of ε_{22} distribution provides the radial elastogram shown in the current study.

Implementation of the LSME

Equation (1) was numerically solved with an iterative procedure that uses the regularized nonlinear minimization method, known in the literature as the Levenberg–Marquardt (L&M) algorithm (Levenberg 1963; Marquardt 1944). The optical flow equations were used to compute the Jacobian matrix (J) that is required to implement the L&M algorithm. J was derived in Maurice et al. (2004a); at the kth iteration, it can be expressed as:

$$J_k = \begin{bmatrix} \dfrac{\partial I_{Lag}}{\partial \theta_1} & \dfrac{\partial I_{Lag}}{\partial \theta_2} & \cdots & \dfrac{\partial I_{Lag}}{\partial \theta_n} \\ \vdots & \vdots & & \vdots \\ \dfrac{\partial I_{Lag}}{\partial \theta_1} & \dfrac{\partial I_{Lag}}{\partial \theta_2} & \cdots & \dfrac{\partial I_{Lag}}{\partial \theta_n} \end{bmatrix} \qquad (5)$$

In the above equation, θ_i are motion parameters, as given by eqns (3) and (4). J_k is a $m \times n$ matrix, where m is the number of pixels in the ROI and n is the six elements of the affine transformation of eqn (3). To complete, it was demonstrated by Maurice et al. (2004a) that, at the kth iteration, the Jacobian matrix can be implemented as:

$$\frac{\partial I_{Lag}(\vec{\theta}^{k-1})}{\partial \vec{\theta}} \cong \frac{\partial I(\vec{\theta}^{k-1})}{\partial \vec{\theta}} =$$

$$-\left\{ \frac{\partial I}{\partial x}, \frac{\partial I}{\partial x}x, \frac{\partial I}{\partial x}y, \frac{\partial I}{\partial y}, \frac{\partial I}{\partial y}x, \frac{\partial I}{\partial y}y \right\}. \qquad (6)$$

Equation (6) gives the full expression for the six components of the Jacobian matrix J_k, of eqn (5). To implement the LSME method, a 526 μm $\times$ 781 μm (200 samples $\times$ 20 RF lines) measurement window, with 86% axial and 90% lateral overlaps, was used (see Maurice et al. 2004b for more details on the meaning of the measurement window). For the purpose of compensating for strain decay along the radius (Ryan and Foster 1997; Shapo et al. 1996b), the elastograms were postprocessed. They were modulated with a function proportional to the square of the vessel radius. Furthermore, the elastograms were low-pass filtered, using a 500 μm $\times$ 500 μm (6 $\times$ 6 pixels) kernel Gaussian filter. The following section presents results obtained with the proposed method, using data acquired from the excised human carotid artery.
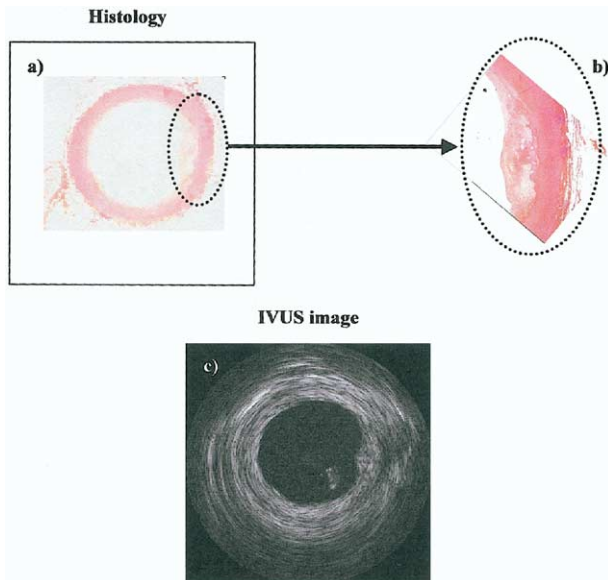
Fig. 2. (a) Histologic section, showing a very thin atherosclerotic plaque at three o'clock; (b) zoom of the atherosclerotic region; (c) log-compressed IVUS image. Notice that the IVUS image does not allow clear differentiation of the plaque from the healthy vascular tissue. Moreover, it offers no possible characterization of the plaque component.

RESULTS

As shown by histology (Fig. 2a and b), the artery was characterized by a thin atherosclerotic plaque (located at three o'clock) that was only restricted to a confined angular sector. The coloration with saffron haematoxylin-eosin revealed that the plaque contained cholesterol crystals and inflammatory cells. Notice that the IVUS image on Fig. 2c does not clearly allow differentiating the plaque from the healthy vascular tissue.

Figure 3 presents 10 elastograms that were computed using the set of 11 RF images acquired for consecutive increasing physiological fluid pressure levels. The elastogram obtained for the lowest intraluminal pressure (i.e., from the first and second RF images, in this case) is displayed in Fig. 3a, whereas Fig. 3j presents the elastogram for the highest pressure difference (i.e., the elastogram computed with the first and eleventh RF images). Indeed, maximum strain values close to 0.6% are observed in Fig. 3a, whereas the maximum is close to 3% in Fig. 3j. To summarize, elastograms in Fig. 3a and j are the least representative and those from Fig. 3c to Fig. 3e present very good plaque detectability, accuracy in plaque dimensions and significant contrast between plaque and surrounding tissue. In other words, a range of intraluminal pressures does exist for which tissue motion estimation appears to be optimal. On the other hand, as can be seen on all panels of Fig. 3, the elastograms presented regions of high strain values at eleven o'clock and, on some, the same observation was noted at seven o'clock.

DISCUSSION

As can be observed in Fig. 2c, IVUS images alone may be insufficient to characterize vascular tissues. EVE was proposed because it may provide quantitative parameters to support the clinicians in diagnosis and prognosis of atherosclerotic evolution. In this paper, an adapted version of the LSME for EVE was experimented in vitro on an excised human carotid artery. Although an optimal range of intraluminal pressures seems to be indicated to improve plaque detectability, the results also showed two specific features. First, comparing elastography with histology, the geometry of the plaque appears to be preserved in the LSME elastograms (mainly in Fig. 3c and d). For instance, the maximum plaque thickness measured in the elastogram of Fig. 3c is close to 360 μm; this estimation is strongly supported by histology measurement conducted by Brusseau et al. (2001), who found a maximum plaque thickness of approximating 350 μm for this very same carotid artery segment. Second, regarding biomechanical properties, a strain ratio close to 3 could be observed between the atherosclerotic plaque and the healthy surrounding vascular tissue for all elastograms presented in Fig. 3. Such information may provide interesting insights about plaque components; it thus may help in predicting plaque rupture and also help in therapy planning. The possibility of assessing quantitative strain values with the LSME may represent a strength of the method.

A major advantage of the LSME over correlation-based techniques (de Korte et al. 1997, 1998, 2000a; Brusseau et al. 2001; Talhami et al. 1994; Ryan and Foster 1997; Shapo et al. 1996b) stems from the fact that it allows computing the full 2-D strain tensor. For instance, complex tissue deformations such as rotation, scaling and shear can appropriately be assessed, whereas they are known to set a potential limitation for correlation-based methods. Although further experiments are required to validate the robustness of the LSME to assess nonrigid motions, our group recently demonstrated with simulations its potential to characterize atherosclerotic plaques that "shelter" lipid pools (potential sites for nonrigid tissue motions) (Maurice et al. 2004a). This can provide important clinical insights, provided that lipid pools are known to have a strong correlation with unstable plaques. On the other hand, the main disadvantage associated with the LSME stems from the fact that its current implementation is time-consuming. Indeed, the method was implemented using the Levenberg–Mar-
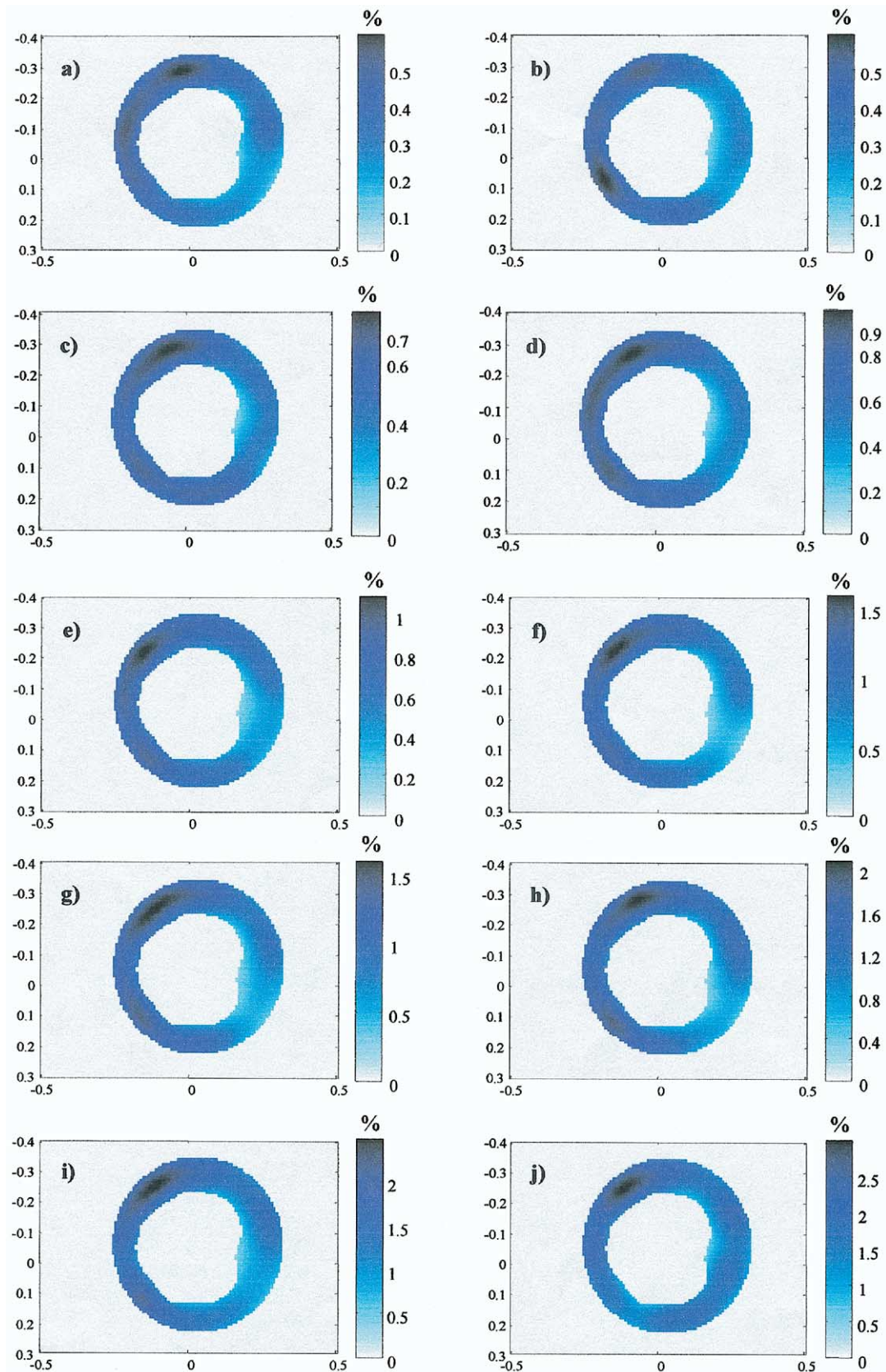
Fig. 3. (a) to (j) Elastograms computed for consecutive increasing physiological fluid pressure levels. Lateral and axial values are dimensions (in cm), and the color scales give the strain in percent.

quardt (L&M) minimization algorithm that requires an iterative process. Nevertheless, our group is currently investigating the optimization of the LSME processing-time.

As seen in Fig. 3, high strain values were noticed at eleven and seven o'clock. It is believed that such a softening artefact more likely relates to the data than to the tissue-motion estimator method. This assumption is based on the fact that the IVUS image (Fig. 2c) also showed some very echogenic signals, specifically at seven o'clock. The exact cause of these high echogenic zones with high strains is unfortunately unknown; they may be related to the tissue preparation.

Finally, it is worthwhile to emphasize the implementation of the optical flow equations to compute the Jacobian matrix in the L&M algorithm (see Maurice et al. 2004a for more details). This likely improves the LSME performance, provided that the optical flow equations better express speckle dynamics than does the finite-difference method that would otherwise be used.

CONCLUSION

In this paper, an in vitro application of the adapted LSME on an excised human carotid artery was investigated. The results clearly demonstrated the potential of the LSME to discriminate between healthy and diseased vascular tissues and, specifically, in this study, to characterize atherosclerotic plaques that appear to be harder than the surrounding vascular tissue. Ten elastograms, for increasing pressure levels, exhibited strong similarities to a continuously increasing strain range, demonstrating the reliability of the estimation process. It was also observed that there might exist a range of intraluminal pressures for which plaque detectability is optimal in the elastograms. In summary, these results give confidence in the adapted LSME to provide accurate geometric and biomechanical parameters that might improve clinicians' diagnosis and prognosis of atherosclerosis evolution.

REFERENCES

Brusseau E, Fromageau J, Finet G, Delachartre P, Vray D. Axial strain imaging of intravascular data: Results on polyvinyl alcohol cryogel phantoms and carotid artery. Ultrasound Med Biol 2001;27(12):1631–1642.

Davies JM, Thomas AC. Plaque fissuring: The cause of acute myocardial infarction, sudden ischaemic death, and crescendo angina. Br Heart J 1985;53:363–373.

de Korte CL, Céspedes EI, Van der Steen AFW, Lancée CT. Intravascular elasticity imaging using ultrasound—Feasibility studies in phantoms. Ultrasound Med Biol 1997;23(5):735–746.

de Korte CL, Pasterkamp G, Van der Steen AFW, Woutman HA, Bom N. Characterization of plaque components with intravascular ultrasound elastography in human femoral and coronary arteries in vitro. Circulation 2000a;102(6):617–623.

de Korte CL, Van der Steen AFW, Céspedes EI, Pasterkamp G. Intravascular ultrasound elastography in human arteries: Initial experience in vitro. Ultrasound Med Biol 1998;24(3):401–408.

de Korte CL, Van der Steen AFW, Céspedes EI, Pasterkamp G, Carlier SG, Mastik F, Schoneveld AH, Serruys PW, Bom N. Characterization of plaque components and vulnerability with intravascular ultrasound elastography. Phys Med Biol 2000b;45(6):1465–1475.

Delachartre P, Cachard C, Finet G, Gerfault L, Vray D. Modeling geometric artefacts in intravascular ultrasound imaging. Ultrasound Med Biol 1999;25(4):567–575.

Falk E. Morphologic features of unstable atherosclerotic plaques underlying acute coronary syndromes. Am J Cardiol 1989;63(Suppl. E):114E–120E.

Falk E. Why do plaques rupture? Circulation 1992;86(Suppl. III):30–42.

Fisher A, Gustein DE, Fayad ZA, Fuster V. Predicting plaque rupture: Enhancing diagnosis and clinical decision-making in coronary artery disease. Vasc Med 2000;5:163–172.

Fung YC. Biomechanical properties of living tissues. 2nd ed. New York: Springer Verlag, 1993:568.

Levenberg K. A method for the solution of certain non-linear problems in least-squares. Q Appl Math 1963;2(2):164–168.

Marquardt DW. An algorithm for least-squares estimation of non-linear parameters. J SIAM 1944;11(2):431–441.

Maurice RL, Bertrand M. Lagrangian speckle model and tissue-motion estimation theory. IEEE Trans Med Imaging 1999;18(7):593–603.

Maurice RL, Ohayon J, Finet G, Cloutier G. Adapting the Lagrangian speckle model estimator for endovascular elastography: Theory and validation with simulated radio-frequency data. J Acoust Soc Am 2004a;116(2):1276–1286.

Maurice RL, Ohayon J, Frétigny Y, Bertrand M, Soulez G, Cloutier G. Non-invasive vascular elastography: Theoretical framework. IEEE Trans Med Imaging 2004b;23(2):164–180.

Ohayon J, Teppaz P, Finet G, Rioufol G. In-vivo prediction of human coronary plaque rupture location using intravascular ultrasound and the finite element method. Coronary Artery Dis 2001;12:655–663.

Ryan LK, Foster FS. Ultrasonic measurement of differential displacement strain in a vascular model. Ultrason Imaging 1997;19(1):19–38.

Shapo BM, Crowe JR, Erkamp R, Emelianov SY, Eberle MJ, O'Donnell M. Strain imaging of coronary arteries with intraluminal ultrasound: Experiments on an inhomogeneous phantom. Ultrason Imaging 1996a;18(3):173–191.

Shapo BM, Crowe JR, Skovoroda AR, Eberle MJ, Cohn NA, O'Donnell M. Displacement and strain imaging of coronary arteries with intraluminal ultrasound. IEEE Trans Ultrason Ferroelec Freq Control 1996b;43(2):234–246.

Talhami HE, Wilson LS, Neale ML. Spectral tissue strain: A new technique for imaging tissue strain using intravascular ultrasound. Ultrasound Med Biol 1994;20(8):759–772.

Zaman AG, Helft G, Worthley SG, Badimon JJ. The role of plaque rupture in coronary artery disease. Atherosclerosis 2000;149:251–266.